Journal of Catalysis **194,** 373–384 (2000)
doi:10.1006/jcat.2000.2940, available online at http://www.idealibrary.com on IDEAL®

Oxidative Steam Reforming of Methanol over CuZnAl(Zr)-Oxide Catalysts for the Selective Production of Hydrogen for Fuel Cells: Catalyst Characterization and Performance Evaluation

S. Velu,* K. Suzuki,*,[1] M. Okazaki,† M. P. Kapoor,‡ T. Osaki,* and F. Ohashi*

*Ceramics Technology Department and †Chemistry Department, National Industrial Research Institute of Nagoya, 1-1 Hirate-cho, Kita-ku, Nagoya 462-8510, Japan; and ‡Department of Energy and Environment, Osaka National Research Institute, 1-8-31, Midorigaoka, Ikeda, Osaka 563-8577, Japan

Received February 15, 2000; revised May 24, 2000; accepted May 31, 2000

A new series of CuZnAl(Zr)-oxide catalysts were prepared by the decomposition of CuZnAl(Zr)-hydroxycarbonate precursors containing hydrotalcite (HT)-like layered double hydroxide (LDH)/aurichalcite phases around 450°C. The physicochemical properties of the catalysts were investigated by X-ray diffraction (XRD), UV–vis diffuse reflectance spectroscopy (DRS), temperature-programmed reduction (TPR), electron paramagnetic resonance (EPR) spectroscopy, and surface area measurements. XRD of the catalysts indicated the presence of a mixture of poorly crystallized CuO and ZnO phases whose crystallinity increased with decreasing Al content. TPR results demonstrated that substitution of Zr for Al improved the copper reducibility and dispersion. UV–vis DRS and EPR results revealed that isolated Cu^{2+} ions interacting with Al were formed in the Al-rich samples, while mostly bulk-like or cluster-like Cu^{2+} species were present in the Zr-rich samples. The oxidative steam reforming of methanol reaction was performed over these catalysts in the temperature range 180° to 290°C at atmospheric pressure using H_2O/CH_3OH, molar ratio = 3. Initially, the Cu : Zn : Al metallic composition was optimized and it was found that catalytic performance in terms of methanol conversion and H_2 production rate increased with decreasing Al content. Among CuZnAl-oxide catalysts the one with Cu : Zn : Al = 37.6 : 50.7 : 11.7 (wt%) was found to be the most active. Replacement of Al either partially or completely by Zr further improved the catalytic performance. The higher catalytic performance of Zr-containing catalysts was attributed to the improved Cu reducibility, higher Cu metal surface area, and dispersion. Studies of the effect of MeOH contact time on the catalytic performance over a Zr-containing catalyst revealed that both CO and CO_2 were produced as primary products, and CO was subsequently transformed into $CO_2 + H_2$ by the water–gas shift reaction/and CO oxidation.

Key Words: **H_2 production; steam reforming of methanol; partial oxidation of methanol; CuZnAl-oxide catalysts; CuZnZr-oxide catalysts; hydrotalcite-like compounds.**

INTRODUCTION

Scientific evidence strongly suggests that the rapid build-up of greenhouse gases in the atmosphere is raising the Earth's temperature (global warming) and changing the Earth's climate with many potential consequences (1). Carbon dioxide (CO_2) emissions from anthropogenic sources are the largest contributor (63.5%) to global warming. Among various anthropogenic sources, transportation now accounts for 23% of global CO_2 emissions; industry, 25%; electric power generation, 34%; and residential/commercial use, 18%. Efforts are currently under way to reduce CO_2 emissions from the transportation sector by the use of hydrogen (H_2) fueled fuel cells such as the polymer electrolyte membrane fuel cell (PEMFC) for powering vehicles (2). Ideally, vehicles would store hydrogen fuel onboard in high-pressure tanks. However, because current technology does not permit storage of enough H_2 to deliver the driving range to which motorists are accustomed, hydrogen may initially be supplied from liquid fuels such as methanol.

For the purpose of fuel-cell applications, H_2 can be extracted from methanol through two different processes (3–6): (i) steam reforming of methanol (SRM) and (ii) Partial oxidation of methanol (POM). Unfortunately, both of these reactions produce a considerable amount of CO as a byproduct. For the application of PEMFC, even traces of CO (>20 ppm) in the reformed gas deteriorate a Pt electrode and the cell performance is lowered dramatically (7). Second stage or multistage catalytic reactors are being used to remove the CO by the water–gas shift (WGS) reaction, CO oxidation, or the methanation reaction. However, the use of additional steps for fuel gas refinement would lower the total efficiency of the propulsion system (8). Hence, in order to utilize hydrogen fuel for fuel cells, it is highly desirable to develop a process that can produce hydrogen without CO in the reformed gas. The reactions are as

[1] To whom correspondence should be addressed. E-mail: ksuzuki3@nirin.go.jp.

0021-9517/00 $35.00

follows:

$$\text{(SRM)}\ CH_3OH + H_2O \Leftrightarrow 3H_2 + CO_2;\quad \Delta H = +49.4\ \text{kJ mol}^{-1} \qquad [1]$$

$$\text{(POM)}\ CH_3OH + 1/2O_2 \Leftrightarrow 2H_2 + CO_2;\quad \Delta H = -192.2\ \text{kJ mol}^{-1} \qquad [2]$$

$$\text{(WGS)}\ CO + H_2O \Leftrightarrow H_2 + CO_2;\quad \Delta H = -39.4\ \text{kJ mol}^{-1}. \qquad [3]$$

We have recently demonstrated that a combined steam reforming–partial oxidation of methanol, termed an "oxidative steam reforming of methanol" (OSRM) reaction over a series of CuZnAl(Zr)-oxide catalysts derived from CuZnAl(Zr)-hydroxycarbonates containing hydrotalcite (HT)/aurichalcite phases offered CO-free hydrogen with methanol conversion above 90% at around 230°C (9). In this paper, we present our detailed investigation of the OSRM reaction over these CuZn-based catalysts together with their physicochemical properties as determined by XRD, UV–vis DRS, TPR, and EPR spectroscopic measurements.

EXPERIMENTAL METHODS

Characterization of Catalysts

Details concerning the catalyst preparation, chemical analyses, XRD, TPR, and N_2 adsorption–desorption studies were reported recently (9–12). The copper surface areas, dispersions, and crystallite sizes were determined by the TPR N_2O passivation method as described in the literature (13, 14). The UV–vis DR spectra of the catalysts as well as of the catalyst precursors were recorded using a Perkin–Elmer UV–vis Spectrometer coupled with a Labsphere RSA-PE-18 reflectance spectroscopy accessory. The samples were diluted (20 wt%) in $MgCO_3$, which was used as a reference in the present study. The spectra were recorded in air at room temperature and data were automatically transferred according to the Kubelka–Munk equation: $f(R) = (1 - R_\infty)^2/2R_\infty$. EPR spectra of all the samples were obtained using a JEOL EPR spectrometer (JES-RE1XM) operating in the X-band region. The amplitude of 100-kHz magnetic field modulation was 0.5 mT, and the microwave power was 1.0 mW throughout the experiment. Observation was made either at room temperature (≈298 K) or at 77 K. In both cases the sample (around 40 mg) in a 4-mm o.d. quartz tube was set in a quartz Dewar vessel which was set in the EPR cavity. All the data were digitized and stored in a computer as a 1.0-Kword file.

Activity Measurements

The oxidative steam reforming of methanol reaction was performed in a conventional fixed-bed flow reactor (4 mm i.d.) using 100 mg of the catalyst (particle size 0.30–0.355 mm) in the temperature range from 180 to 290°C at atmospheric pressure. The catalyst was first reduced in a stream of H_2 (10–20 cc/min) from room temperature to 300°C with a heating rate of 5°C/min and dwelled at this temperature for 3 h before cooling to the reaction temperature. Subsequently, premixed water and methanol with H_2O/CH_3OH molar ratio 1.3 were fed into the preheater by means of a microfeeder (liquid flow rate 2.5 cc/h). Synthetic air (20.2 vol.% of O_2 in N_2) at a rate of 10 to 20 cc/min and Ar (carrier gas, 43 cc/min) were adjusted by means of a mass flow controller. The reaction products were analyzed on-line using two gas chromatographs (Shimadzu GC-8A and GL Sciences, Japan GC-320) equipped with thermal conductivity detectors. The GC-8A, equipped with a 2-m long Porapak-Q column, was able to detect the liquid products such as water, methanol, formaldehyde, methyl formate, and dimethyl ether. The gaseous products such as H_2, air, CO, CO_2, and CH_4 were detected by the GC-320 equipped with an activated carbon column. GC peak areas for CO were calibrated using 100 and 10,000 ppm CO in N_2 gas available commercially (Takachiho Trading Co., Ltd., Japan). Under the experimental conditions the CO detection limit of the GC-320 was ca. 700 ppm with ±2% accuracy. In order to determine the level of CO accurately in ppm, the effluent of the GC-320 was also passed through a methanizer and a third GC (GL Sciences, Japan) equipped with a flame ionization detector (FID). The CO detection limit of the methanizer and FID-GC assembly was well below 10 ppm. The catalytic activity was evaluated from the data collected between hours 5 and 6 of the reaction. The stability of the catalyst was examined during 25 h of on-stream operation at 230°C.

RESULTS AND DISCUSSION

Catalyst Characterization

XRD and chemical analyses. The chemical compositions and XRD phases of the CuZnAl(Zr)-oxide catalyst precursors are gathered in Table 1, while the XRD patterns of a few representative samples are illustrated in Fig. 1. A Cu content of 35–40 wt% has been maintained in all the samples while the (Cu + Zn)/(Al + Zr) ratio has been varied. This is because earlier studies (3, 15) have demonstrated that a Cu–Zn catalyst containing 30–40 wt% Cu was the most active for the POM/SRM reactions. Al was partially replaced by Zr in the sample CZAZP-6, while in CZAZP-7 it was completely replaced by Zr. The XRD patterns of the uncalcined samples (See Fig. 1, top) exhibit hydroxy carbonates containing hydrotalcite (HT)-like layered double hydroxide (LDH; JCPDS file No. 38-487) as a primary phase (10). The purity of the phase, however, depends on the (Cu + Zn)/(Al + Zr) atomic ratio. As the Al content in the sample decreases other phases such as aurichalcite

TABLE 1

Chemical Compositions and XRD Phases of CuZnAl(Zr)-Oxide Catalyst Precursors

Precursor	Metal composition (wt%)[a]				(Cu + Zn)/(Al + Zr) atomic ratio[a]	XRD phase obtained
	Cu	Zn	Al	Zr		
CZAZP-1	35.3	44.1	20.6	0.0	1.61	LDH
CZAZP-2	36.7	48.0	15.3	0.0	2.32	LDH + AH + AC
CZAZP-3	39.3	48.9	11.8	0.0	3.17	LDH + AH + AC
CZAZP-4	37.6	50.7	11.7	0.0	3.31	LDH + AH + AC
CZAZP-5	37.9	53.0	9.1	0.0	4.18	LDH + AH + AC
CZAZP-6	35.9	44.7	5.1	14.3	3.59	AC + LDH + AH
CZAZP-7	32.3	40.5	0.0	27.2	3.79	AC

Note. LDH, layered double hydroxide [$(CuZn)_6Al_2(OH)_{16}CO_3 \cdot 4H_2O$], JCPDS file 38-487; AH, $Al(OH)_3$ (bayerite), JCPDS file 20-11; AC, aurichalcite [$(Zn,Cu)_5(CO_3)_2(OH)_6$], JCPDS file 7-743.

[a] Chemical analyses results obtained from XRF spectroscopy.

($(Cu,Zn)_5(CO_3)_2(OH)_6$; JCPDS file No.7-743) and bayerite ($Al(OH)_3$; JCPDS file No.20-11) are also noticed, besides the LDH phase. The sample CZAZP-7 without Al exhibited aurichalcite as a single phase. Thermal decomposition of these hydroxycarbonate precursors at 450°C/5 h results in the formation of a mixture of poorly crystallized CuO and ZnO phases (see Fig. 1, bottom). Other phases containing Cu/Zn/Al are more likely to be present, but because of their poor and highly disordered crystallization they could not be detected by the XRD. The crystallinity of the phase increases with increasing (Cu + Zn)/(Al + Zr) atomic ratio (see Table 1). It is interesting to note that the presence of a mixture of CuO and ZnO can be clearly discerned in the Zr-containing samples. These calcined samples have been employed as catalysts for the SRM and OSRM reactions in the present study. The CuO phase is reduced to metallic copper upon H_2 reduction up to 300°C.

Table 2 summarizes the physicochemical properties of the CuZnAl(Zr)-oxide catalysts. The BET surface areas, the specific pore volumes and pore radii of unreduced samples, and the copper surface areas, dispersions, and particle sizes of reduced samples depend on the Cu : Zn : Al : Zr chemical composition in the precursor. It can be seen that catalysts containing Zr exhibit higher copper surface areas and copper dispersions than those without Zr (Al-containing analogues).

UV–vis diffuse reflectance (DR) spectroscopy. The UV–vis DR spectra of both uncalcined and calcined samples were recorded because the blue color of the uncalcined samples transformed into dark green or black upon calcination depending on the (Cu + Zn)/(Al + Zr) ratio. For comparison, the DR spectra of pure ZrO_2 and CuO reference samples were also recorded. Pure ZrO_2 exhibits (Fig. 2) a characteristic band around 220 nm due to the $O_2^{2-} \rightarrow Zr^{4+}$ charge transfer transition (16). The standard sample of CuO shows a strong band around 800 nm which is due to the $^2Eg \rightarrow {}^2T_2g$ transition of Cu^{2+} in the octahedral symmetry (17). The CuZnAl(Zr)-hydroxycarbonate precursors also

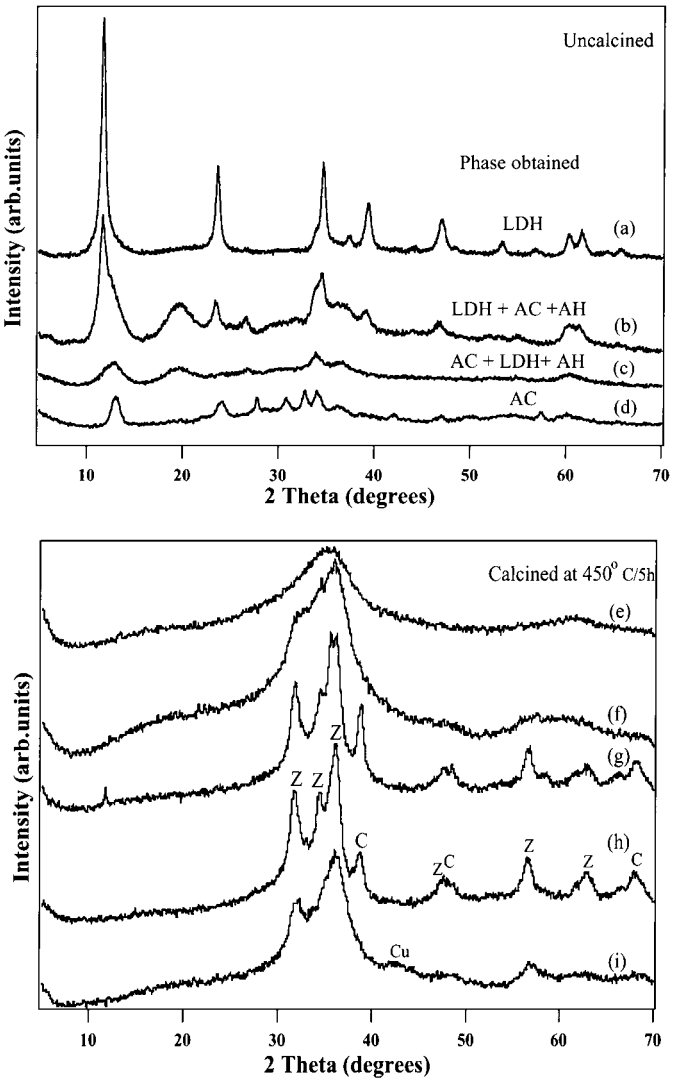

FIG. 1. XRD patterns of CuZnAl(Zr)-oxide catalyst precursors (top) and those of catalysts (bottom): (a) CZAZP-1, (b) CZAZP-4, (c) CZAZP-6, (d) CZAZP-7, (e) CZAZOC-1, (f) CZAZOC-4, (g) CZAZOC-6, (h) CZAZOC-7, (i) CZAZOC-4 reduced in the reactor using H_2 stream. C = CuO and Z = ZnO phases.

TABLE 2

Physicochemical Properties of CuZnAl(Zr)-Oxide Catalysts

Catalyst	Physicochemical properties[a]					
	S_{BET} ($m^2\ g^{-1}$)	Pore volume ($cc\ g^{-1}$)	Pore radius (Å)	S_{cu} ($m^2\ g^{-1}$)	D_{cu} (%)	t_{Cu} (Å)
CZAZOC-1	56	0.181	98	203	38.6	26
CZAZOC-2	71	0.263	93	181	34.3	29
CZAZOC-3	84	0.406	60	176	33.4	30
CZAZOC-4	108	0.428	80	227	43.1	23
CZAZOC-5	54	0.130	20	190	40.0	25
CZAZOC-6	65	0.172	40	232	44.0	23
CZAZOC-7	59	0.099	20	279	52.9	19

[a] Cu surface area (S_{cu}), Cu dispersion (D_{cu}), and Cu particle sizes (t_{Cu}) were determined by TPR-N_2O passivation method.

show a band around 800 nm. However, this band is very broad and weak compared to that of the pure CuO, probably because of the distortion of the octahedral symmetry. Hence, this broad band can be assigned to the envelope of the $d_{z^2} \rightarrow d_{x^2-y^2}$, $d_{xz,yz} \rightarrow d_{x^2-y^2}$, and $d_{xy} \rightarrow d_{x^2-y^2}$ transitions that occur when Cu^{2+} ions are in a distorted octahedral symmetry (18). The strong band around 240 nm in both CZAZP-3 and CZAZP-7 samples can be attributed to the $O^{2-} \rightarrow Cu^{2+}$ ligand to metal charge transfer (LMCT) transition.

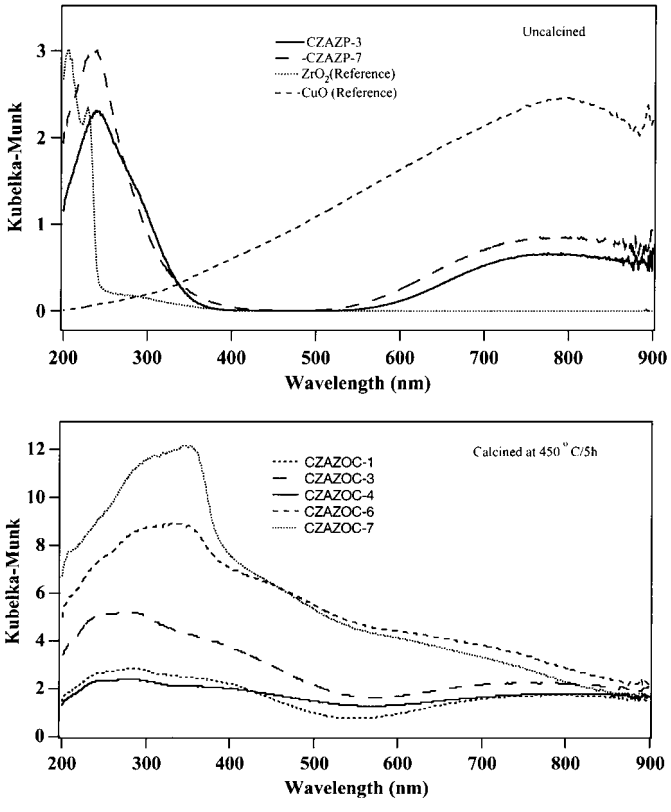

FIG. 2. UV–vis diffuse reflectance spectra of (top) CuZnAlZr-oxide catalyst precursors and (bottom) those of catalysts.

The DR spectra of calcined samples show two main bands; one between 240 and 400 nm and the other around 700 nm together with several shoulders. The band around 800 nm corresponding to the Cu^{2+} in the octahedral coordination is very broad in the calcined samples suggesting a further distortion in the symmetry of the copper environment. According to an earlier report (19), a band around 700 nm and a stronger absorption band between 250 and 290 nm characterized copper–alumina samples. The former has been attributed to the $^2Eg \rightarrow {}^2T_2g$ spin-allowed transition of Cu^{2+} ions in the distorted octahedral environment of the surface alumina sites with a spinel-type structure. The characteristic band around 400 nm for ZnO, which is absent in the uncalcined samples appears as a shoulder in the calcined samples, indicating the formation of ZnO phase along with CuO phase as evidenced by the XRD data (see Fig. 1, bottom). A closer observation reveals significant differences between Al-containing samples and the Zr-containing samples in the DR spectra. For example, the Kubelka–Munk function increases with increasing Zr content (decreasing Al content) in the Zr-containing sample. These samples exhibit a broad band between 300 and 350 nm together with a shoulder superimposed on the band between 600 and 800 nm. These bands are attributed to the charge transfer involving Cu^{2+}–O^{2-}–Cu^{2+} species, possibly a cluster-like or bulk-like species. It should, however, be noted that a band around 450 nm in the degassed Cu/Al_2O_3 system has been assigned to the formation of Cu^+ three-dimensional clusters in the CuO matrix (20). Although the DR spectra in the present study has been recorded in air atmosphere, the formation of such Cu^+ species in the Zr-containing samples cannot be discarded. In the Al-containing samples, on the other hand, bands around 300–350 nm and a shoulder around 450 nm are very weak. Also, the LMCT transition band is shifted toward a lower wavelength (250–300 nm). It can be concluded from the DRS results that bulk-like or cluster-like Cu^{2+} species or Cu^+ three-dimensional clusters are formed upon calcination of Zr-containing catalyst precursors. In contrast, relatively isolated Cu^{2+} ions are present in the Al-containing samples.

Temperature programmed reduction (TPR). The reducibility of copper species in the CuZnAl(Zr)-mixed oxide catalysts was investigated by TPR experiments and the profiles are displayed in Fig. 3. All the samples exhibit a broad reduction profile together with shoulders in the temperature range 200–300°C. In order to get more insight into the TPR results the profiles are deconvoluted using a computer program (12). The peak positions and their contributions derived from deconvolution are summarized in Table 3. The original TPR profile can be deconvoluted into at least three peaks in all cases. It is interesting to note that the copper reducibility depends on the Al and/or Zr content in the

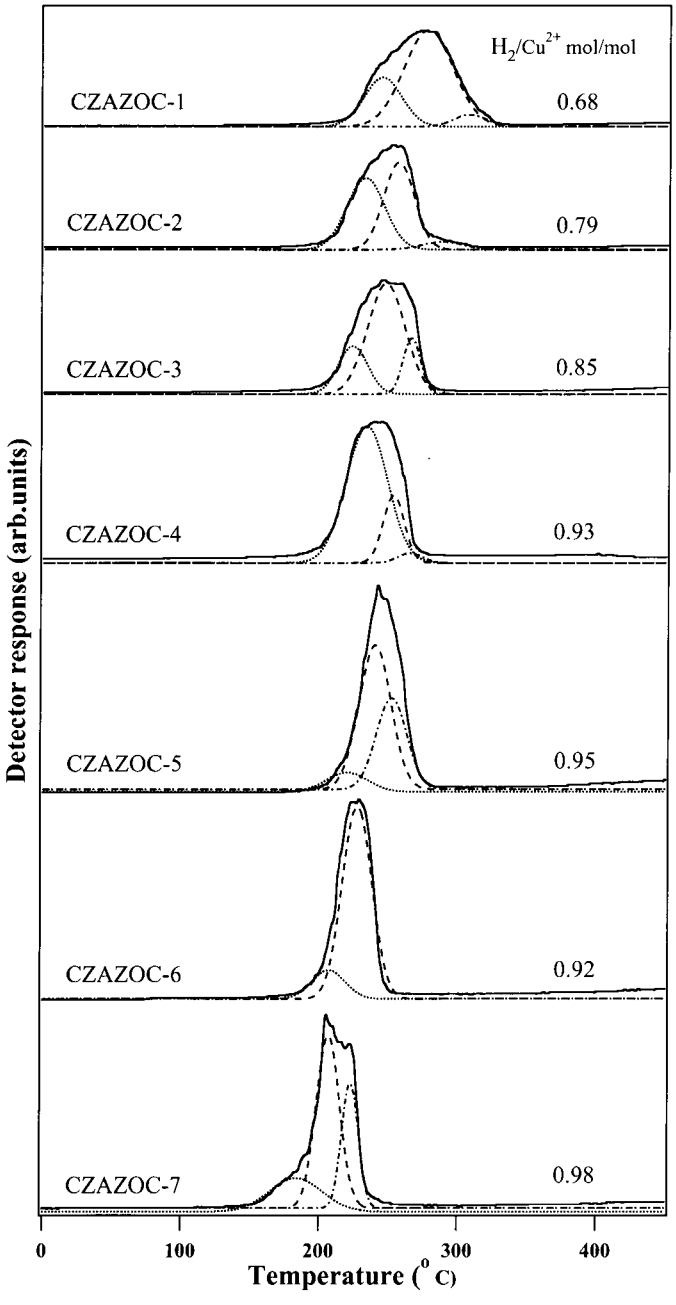

FIG. 3. TPR profiles of CuZnAl(Zr)-oxide catalysts. Solid lines are experimental curves and dotted/broken lines are deconvoluted curves.

sample despite the fact that the Cu content in all the samples was kept almost constant (35–40 wt% = 30–35 mol%) by varying the Zn, Al, and Zr content (see Table 1). For instance, the TPR reduction peak is very broad and the extent of reduction (H_2/Cu^{2+} molar ratio) is the lowest (0.68) for CZAZOC-l catalyst. The reduction peak is shifted toward low temperatures and peaks become relatively sharp with decreasing Al content. This may be because of the lower crystallinity of CuO in those samples with higher Al content, as evidenced from XRD results (Fig. 1). It is also possible that the surface spinel specie, i.e., $CuAl_2O_4$, can be easily formed in samples with higher Al content, which would get reduced at relatively high temperatures compared with CuO. This would result in the appearance of a broad TPR profile, which upon deconvolution produces peaks at higher temperatures (peak 3 in CZAZOC-1 to CZAZOC-3). The sample CZAZOC-7 without Al exhibits the lowest onset temperature of around 160°C. The first peak is centered at around 184°C and the reduction is completed around 240°C itself. These results reveal that a decrease in Al content improves the copper reducibility. Alternatively, substitution of Zr for Al enhances the copper reducibility.

TPR reoxidation experiments. As discussed above, the TPR profiles of CuZnAl(Zr)-oxide catalysts are very broad. In order to confirm that there is a saturated phenomenon for certain copper species, we performed reoxidation experiments on a few representative samples, namely the catalyst containing higher amounts of Al (CZAZOC-1), the catalyst containing both Al and Zr (CZAZOC-6), and the catalyst containing only Zr without Al (CZAZOC-7). This experiment is similar to that of N_2O passivation used in the determination of copper metallic surface areas (10, 13). Briefly, a normal TPR of the fresh (calcined) catalyst was recorded first. The reduced catalyst was reoxidized for about 2 h at various temperatures, viz. 75, 150, and 300°C, using molecular oxygen (O_2 gas, flow rate ≈20 cc/min), and then brought down to room temperature. The oxidized catalyst was again subjected to the second TPR. Fresh samples were employed for reoxidation at each temperature. He gas (flow rate ≈30 cc/min) was used to flush out the residual H_2 or O_2 in each step of the experiment. The H_2/Cu^{2+} molar ratio represents the extent of reoxidation at each temperature. The reoxidation causes the supported copper oxide species to be redispersed on the support depending upon the extent of the interaction between copper metal and the support (ZnAl-oxide or ZnAlZr-oxide).

TABLE 3

TPR Peak Positions and Concentrations of Reducible Species in the CuZnAl(Zr)-Oxide Catalysts as Determined by the Deconvolution of TPR Profiles

Catalyst	TPR peak position [temperature (°C)] and concentration (%)[a]		
	Peak 1	Peak 2	Peak 3
CZAZOC-1	244 (26.4)	277 (68.0)	307 (5.6)
CZAZOC-2	232 (47.4)	256 (47.0)	288 (5.6)
CZAZOC-3	223 (21.5)	247 (63.4)	266 (15.1)
CZAZOC-4	233 (77.2)	253 (19.6)	265 (3.2)
CZAZOC-5	220 (9.7)	240 (56.1)	252 (34.2)
CZAZOC-6	207 (14.4)	227 (85.6)	—
CZAZOC-7	184 (22.5)	207 (51.5)	223 (26)

[a] Values in parentheses are the contribution (%) of each species.

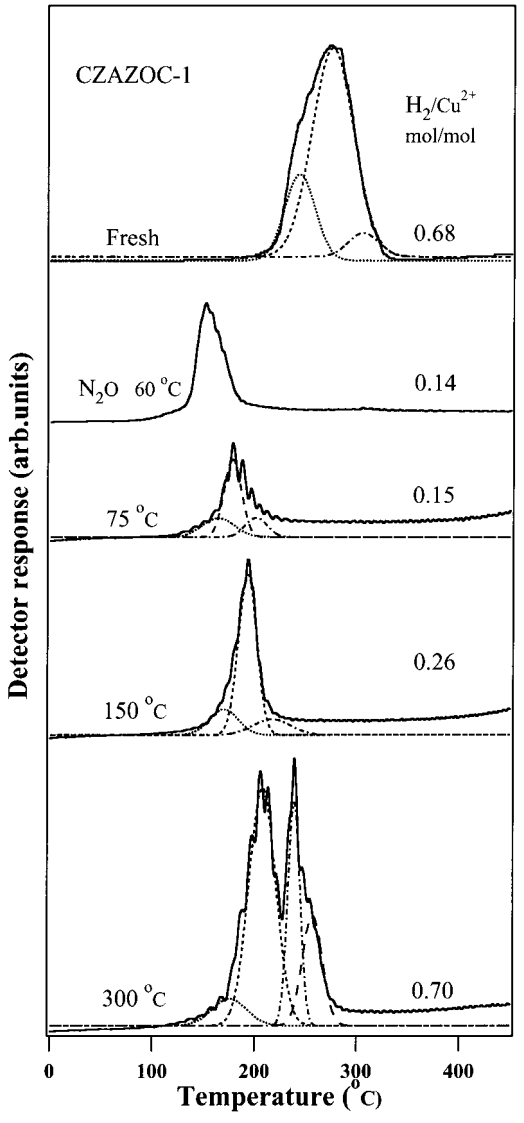

FIG. 4. TPR profiles of CZAZOC-1 obtained in the reoxidation treatment at the indicated temperatures. Solid lines are experimental curves and dotted/broken lines are deconvoluted curves.

The TPR patterns of the reoxidized catalysts CZAZOC-1, CZAZOC-6, and CZAZOC-7 are shown in Figs. 4, 5, and 6, respectively. For comparison, the TPR profiles recorded in the N_2O passivation experiments are also included. The profiles are deconvoluted and the peak positions and quantitative data are collected in Table 4. It can be seen from the figures and table that the TPR patterns and the extent of reoxidation of each sample at each temperature are markedly different, demonstrating that the redispersion of copper species depends on the chemical composition of the support. Reoxidation of CZAZOC-1 and CZAZOC-7 at 75°C produces more or less similar TPR profiles. On the other hand, the reoxidation of CZAZOC-6 produces a relatively broad peak, which could be deconvoluted into at least four peaks. It has been assumed that the reoxidation of these Cu-based catalysts using N_2O resulted in the oxidation of only surface copper atoms to Cu^+ (13, 14). Hence, it may be reasonable to state that mainly surface copper atoms are being oxidized during reoxidation of CZAZOC-1 and CZAZOC-7 at 75°C while in addition to the surface copper atoms a part of bulk copper atoms are also oxidized in CZAZOC-6. Reoxidation at 150°C produces a relatively sharp peak, with much less extent of reoxidation of 0.26 for the sample CZAZOC-1. In contrast, a doublet with a larger extent of reoxidation above 0.60 is obtained for samples CZAZOC-6 and CZAZOC-7. These results imply that the higher the Al content, the lower the reoxidability of copper catalysts that can be observed. In all cases, although the original TPR profiles of fresh catalysts exhibit a single broad reduction peak, the reoxidation at 300°C results

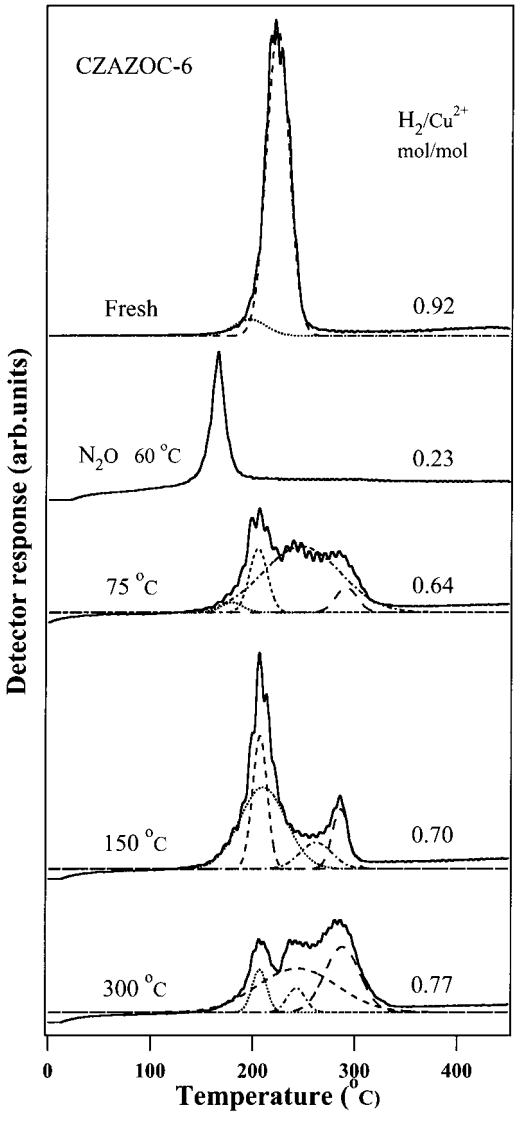

FIG. 5. TPR profiles of CZAZOC-6 obtained in the reoxidation treatment at the indicated temperatures. Solid lines are experimental curves and dotted/broken lines are deconvoluted curves.

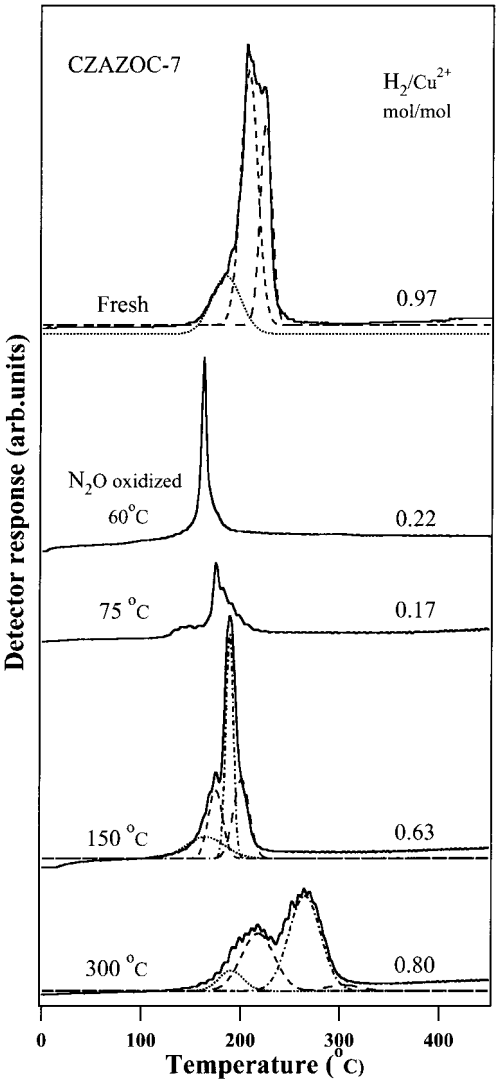

FIG. 6. TPR profiles of CZAZOC-7 obtained in the reoxidation treatment at the indicated temperatures. Solid lines are experimental curves and dotted/broken lines are deconvoluted curves.

in the appearance of at least a doublet with several shoulders. This is because of the redispersion of the copper species on the support during reoxidation experiments. This also causes a shift of the peak positions depending upon the extent of interaction between copper and the support. For instance, the TPR profile in the Al-rich sample is shifted toward lower temperature and the extent of reoxidation (0.70) is similar to the extent of reduction of the fresh catalyst (0.68). In contrast the profiles are shifted toward higher temperatures in catalysts containing Zr (CZAZOC-6 as well as CZAZOC-7) and the extent of reoxidation is less than the extent of reduction of the fresh catalysts (see Figs. 5 and 6). It is also interesting to note that the overlap of low temperature shoulder peak, which is remarkable in the catalyst CZAZOC-7 centering at around 184°C (Fig. 3), has been distinctly separated by the reoxidation treatment at 300°C. Thus, the TPR reoxidation experiment is very useful in that if there is a shoulder or latent peak in the TPR pattern, its deserved feature can be revealed by the reoxidation treatment due to its different reoxidability (21).

Electron paramagnetic resonance (EPR) spectroscopy. EPR spectroscopic investigations were performed on a few representative catalysts under different experimental conditions namely, under air atmosphere, under vacuum, at room temperature, and at 77 K, in order to understand the nature of copper species and their interactions with supports. Figure 7 represents the EPR spectra of some of these samples. In all instances the spectra showed the presence of two kinds of signals, with signal A exhibiting a resolved hyperfine pattern of four peaks and signal B exhibiting no hyperfine structure. Both signals A and B are typical of Cu^{2+} ions. Signal B showing unresolved hyperfine splitting could be attributed to the Cu^{2+} species interacting with each other and generally referred to as "clustered Cu^{2+} ions." On the other hand, signal A with resolved hyperfine pattern could be interpreted as arising from distorted

TABLE 4

Effect of Reoxidation Temperature on the TPR Peak Positions and Concentrations of Reducible Species in the CuZnAl(Zr)-Oxide Catalysts as Determined by the Deconvolution of TPR Profiles

Catalyst	Reoxidation temperature (°C)	TPR peak position [temperature (°C)] and concentration (%)[a]			
		Peak 1	Peak 2	Peak 3	Peak 4
CZAZOC-1	75	164 (23.2)	178 (51.1)	201 (13.9)	221 (9.8)
	150	170 (17.2)	193 (68.9)	217 (13.9)	—
	300	176 (7.6)	208 (52.2)	239 (22.2)	257 (18.0)
CZAZOC-6	75	179 (3.1)	205 (16.6)	247 (72.6)	291 (7.7)
	150	207 (26.0)	210 (49.8)	262 (11.1)	286 (13.1)
	300	207 (9.2)	243 (6.4)	244 (51.1)	288 (33.3)
CZAZOC-7	150	165 (17.5)	175 (20.5)	189 (35.6)	201 (26.4)
	300	186 (8.9)	213 (33.8)	260 (53.9)	299 (3.4)

[a] Values in parentheses are the contribution (%) of each species.

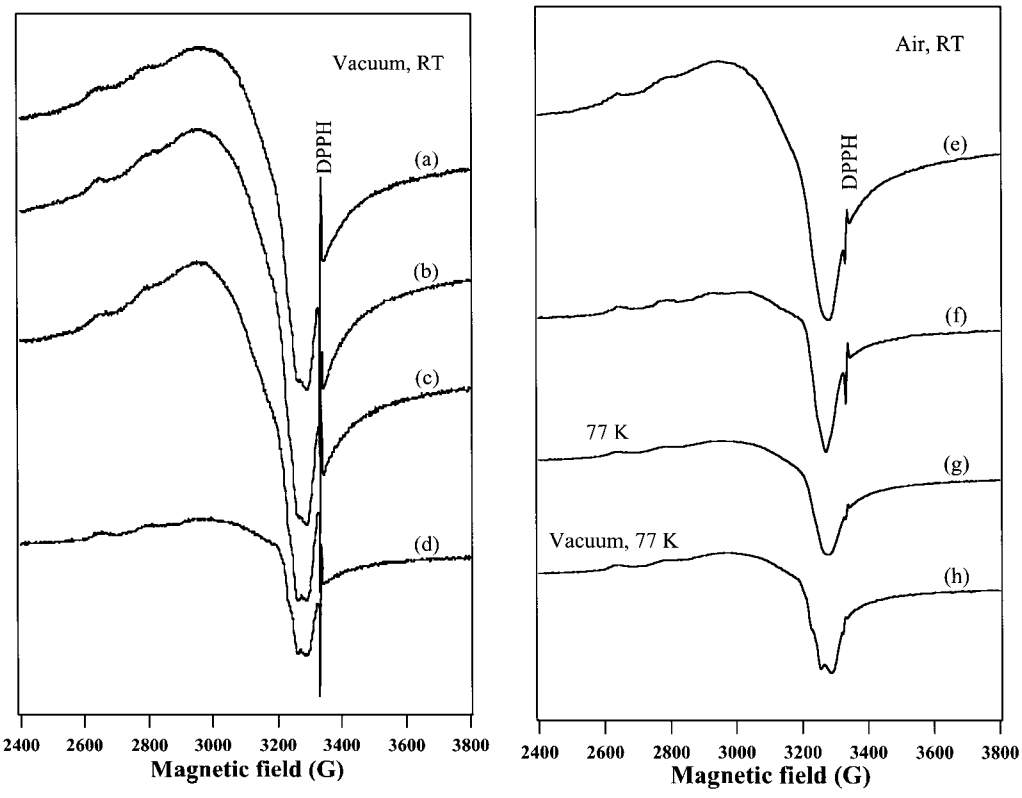

FIG. 7. EPR spectra of CuZnAl(Zr)-oxide catalysts recorded under different experimental conditions: (a) CZAZOC-1, (b) CZAZOC-4, (c) CZAZOC-6, (d) CZAZOC-7 all recorded under vacuum at room temperature (≈298 K), (e) CZAZOC-1, (f) CZAZOC-7 both recorded under air atmosphere at room temperature, (g) CZAZOC-7 recorded under air at 77 K, and (h) CZAZOC-7 recorded under vacuum at 77 K.

octahedrallycoordinated Cu^{2+} ions (19, 21–23). The four-line hyperfine splitting is typical of isolated Cu^{2+} ions in an axial environment and shows a hyperfine structure better resolved in the $g_{\|}$ component. A closer inspection of the spectra revealed that the hyperfine structure of the $g_{\|}$ components is due to the superimposition of two sets of four hyperfine lines. The EPR parameters of the paramagnetic components employed in the simulation of experimental spectra are reported in Table 5. The presence of two sets of EPR signals, namely component 1 and component 2, reveals that there are two slightly different kinds of copper ions in the system. The component 2 signal, which is characterized by a higher $g_{\|}$ and lower $A_{\|}$ values, corresponds to Cu^{2+} species undergoing a more marked axial interaction than that of component-1 species (22).

TABLE 5

EPR Parameters of Paramagnetic Components Employed in the Simulation

Component	*g* value		Hyperfine coupling constant (G)	
	$g_{(\|)}$	$g_{(\perp)}$	$A_{(\|)}$	$A_{(\perp)}$
Component 1	2.323	2.065	153	35
Component 2	2.343	2.070	144	15

It is also noticed that, in all cases, the EPR signals did not recover the baseline, suggesting a large contribution of a broad component. Another interesting feature noticed from the EPR spectra is that the EPR signal intensity (amplitude) is strongly influenced by the chemical compositions. For instance, the signal amplitude around 3000 G is diminished to a great extent and the overall intensity is reduced to about threefold when Zr replaces Al in the sample (compare curves (b) and (d)). It should be mentioned that the signal intensity of the EPR is proportional to the spin concentration of the isolated Cu^{2+} ion (20). Hence, the reduction in the EPR signal intensity upon substitution of Zr for Al can be attributed to the reduction of the amount of isolated Cu^{2+} ions. As pointed out earlier based on XRD and UV–vis DRS results, amorphous $CuAl_2O_4$ spinel-like species could be present in the Al-containing samples. The signal A in Al-rich sample is therefore due to the isolated Cu^{2+} ions that are interacting with close Al^{3+} ions. In contrast, such amorphous species are absent in the Zr-rich samples, thereby reducing the signal intensity. So the result implies that in the Zr-containing catalysts the copper is present mostly as CuO-like clusters disbursed on the support. Similar results were also observed in the Cu–Zn

mixed oxide systems without Al as well as in the Cu supported on Y stabilized ZrO_2 catalyst (20, 22). The observed differences in EPR patterns between Al-containing samples and Zr-containing samples in the present study leads to the conclusion that the presence of Al in these samples favors the formation of more isolated Cu^{2+} ions that are interacting with Al^{3+}. These isolated Cu^{2+} ions, therefore, would get reduced at relatively higher temperatures, thus exhibiting broad TPR profiles (Fig. 3). In contrast, such isolated Cu^{2+} ions are almost absent in Zr-containing samples. The clustered Cu^{2+} ions can be easily reducible, as evidenced from the TPR results, and thus exhibit higher copper metallic surface areas, metal dispersion, and lower particle sizes compared to those of Al-containing samples (Table 2). The EPR results are therefore inconsistent with XRD, UV–vis, DRS, and TPR results of the present study. It can also be noticed from Fig. 7 that the EPR signal intensity is significantly reduced when the spectra were recorded in the air atmosphere. This result reveals that most of the detected Cu^{2+} ions are located on the surface of the sample (21). On the other hand, the evacuation temperature does not influence the signal intensity much, indicating that the Cu^{2+} species are not reduced during evacuation. However, the signal is broadened when it is recorded at 77 K, indicating the presence of copper ions in more than one chemical environment at low temperature.

Evaluation of Catalytic Performance

OSRM reaction over CuZnAl-oxide catalysts. We have demonstrated recently that a combined steam reforming and partial oxidation reaction termed "oxidative steam reforming of methanol (OSRM)" over CuZnAl(Zr)-oxide catalysts is more efficient for the selective production of H_2 at relatively lower temperatures of around 230°C (9). Under our controlled experimental conditions, the methanol conversion approached around 100% at around 230°C without any detectable CO in the outflow gas stream (within the detection limit of TCD). For the purpose of optimizing better catalytic performance, the OSRM reaction was performed over a series of CuZnAl-oxide catalysts with various (Cu + Zn)/Al atomic ratio and the results are plotted in Fig. 8. It can be seen that the catalytic performance in terms of methanol conversion and the rate of H_2 production increases with decreasing Al content (increasing (Cu + Zn)/Al atomic ratio) in the sample. One of the reasons for this observation could be the formation of aurichalcite phase in addition to the LDH phase in the catalyst precursor with low Al content (Fig. 1 and Table 1). This is in line with an earlier report on the methanol synthesis CuZn-catalysts wherein higher yields of methanol were obtained over a catalyst precursor contained aurichalcite phase (24). However, the catalytic activity in the present study is leveled off with a further increase in the (Cu + Zn)/Al atomic ratio of around 3.3. Hence, among the catalysts tested in

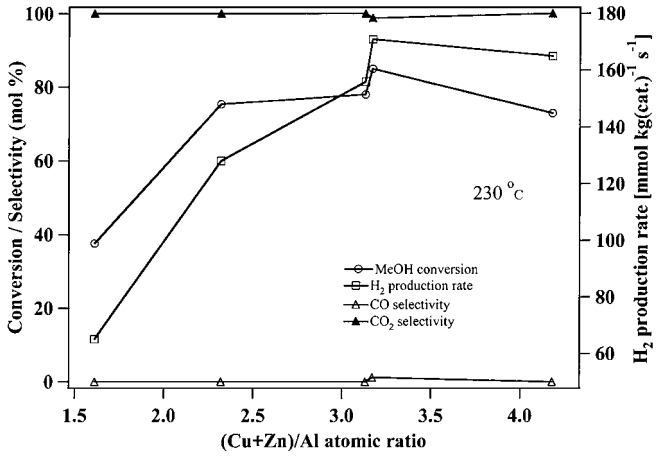

FIG. 8. Effect of (Cu + Zn)/Al atomic ratio on the catalytic performance in the oxidative steam reforming of methanol. Results compared after 25 h of on-stream operation at 230°C.

the present study, the catalyst CZAZOC-4 offers the highest methanol conversion of above 80 mol% with the highest H_2 production rate of about 170 mmol kg(catalyst)$^{-1}$ s^{-1}. The higher catalytic performance of the later catalyst could be attributed to the higher copper surface area and copper dispersion (Table 2). The CO_2 selectivity remained above 99.8% for all the samples, and only traces of CO are recorded under the present experimental conditions (within TCD detection limit).

Effect of substitution of Al by Zr on the catalytic performance. The methanol reforming reaction can be considered as the *reverse* of the methanol synthesis reaction using CO/H_2 or CO_2/H_2 as a feed stock over Cu-based supported catalysts. Among various supports, zirconia emerged as an interesting material for copper catalysts. It is known in the literature that catalysts containing copper and ZrO_2 behave in a bifunctional manner, with copper and ZrO_2 playing complementary but different roles in methanol synthesis reaction (25, 26). A recent report on the detailed *in situ* FTIR investigation of methanol decomposition on the $Cu/ZrO_2/SiO_2$ catalyst revealed the involvement of similar bifunctional roles of copper and ZrO_2 in the methanol decomposition (27). Accordingly, methanol interacts with the OH groups of ZrO_2 to form methoxide and water. The adsorbed methoxide species are dehydrogenated into formaldehyde and subsequently decomposed to gas-phase CO_2 and hydrogen generation. The primary role of copper is to accept the hydrogen released from the surface species located on ZrO_2 and subsequent desorption of molecular hydrogen. Such bifunctional roles of copper and ZrO_2 can also be expected to cause a beneficial change in the synergy between copper and zinc in the CuZnAl-oxide catalysts. Furthermore, ZrO_2 is known to possess oxygen ion vacancy, which causes a geometric effect that can influence the dispersion and alter the morphology of

the supported copper metal particle (21). Taking into account these unique features rendered by the ZrO_2 in the supported catalytic systems, we intended to investigate the effect of addition of Zr in the CuZnAl-oxide catalyst on the catalytic performance in the OSRM reaction. For this purpose, we synthesized two more catalyst samples by replacing Al either partially or completely by Zr in the sample CZAZP-4.

Figure 9 depicts the effect of temperature on the catalytic performance in the OSRM reaction over the CuZn-based catalyst containing Al (CZAZOC-4), the catalyst containing both Al and Zr (CZAZOC-6), and the catalyst containing only Zr without Al (CZAZOC-7). It can be clearly seen that the substitution of Zr for Al improves the catalytic performance in terms of both methanol conversion and H_2 production rate. The catalyst containing Zr without Al exhibit the highest methanol conversion and H_2 production rate throughout the temperature range studied. The higher catalytic performance of the CZAZOC-7 can be accounted for by enhanced copper reducibility, as shown clearly in the TPR studies (Figs. 3–6). It should be recalled that in the methanol synthesis reaction the catalyst involves a Cu^o/Cu_{ox} redox mechanism (28). Hence, the ease of reducibility is likely to be an important factor in determining the efficiency of the catalysts in the reforming reaction. Furthermore, the catalyst CZAZOC-7 exhibits the highest copper surface area and copper metal dispersion and the smallest crystallite size (see Table 2), thereby improving the catalyst synergy between CuZn and Zr. Similar results were also reported very recently in the steam reforming of methanol over Cu/Zn/Zr catalysts with a Cu:Zn:Zr molar ratio of 70:18:12 (6, 29). Although the CO selectivity in the present investigation is slightly higher over CZAZOC-7 it remains low (carbon selectivity up to 1 mol%) in the temperature range studied.

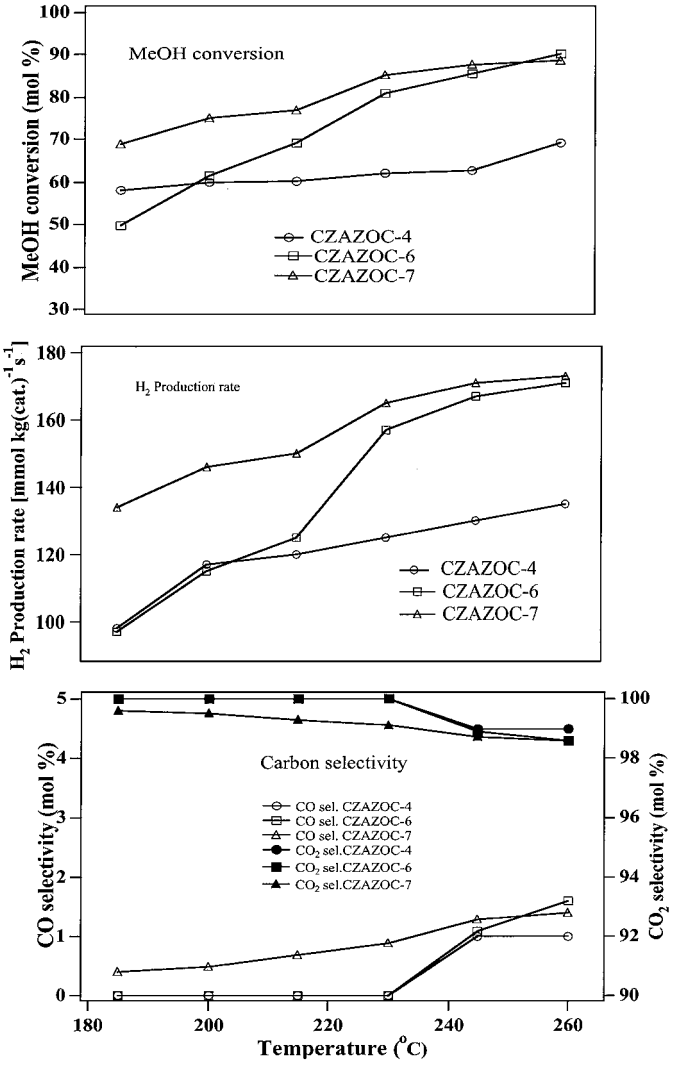

FIG. 9. Effect of temperature on the catalytic performance in the oxidative steam reforming of methanol over CuZn-based catalyst containing only Al (CZAZOC-4), catalyst containing both Al and Zr (CZAZOC-6), and catalyst containing only Zr (CZAZOC-7).

The stability of the catalysts during the OSRM reaction was investigated over 25 h of on-stream operation at 230°C and the results are displayed in Fig. 10. It can be observed that all *three* catalysts tested in the present study exhibit stable activity (within the experimental error of ca. ±5%) in terms of methanol conversion. Although a minor drop in methanol conversion is noticeable over CZAZOC-7, the rates of production of H_2, CO_2, and CO remain unaffected, demonstrating that catalyst deactivation is insignificant. In the case of CZAZOC-4, however, a minor drop in the H_2 production rate is observed during on-stream operation. Since the methanol conversion remains unaffected, the drop in H_2 production rate in this case might be caused by the oxidation of H_2 with O_2 as shown in

$$H_2 + 1/2O_2 \Leftrightarrow H_2O. \qquad [4]$$

In addition, the CO selectivity increases at the expense of the selectivity of CO_2 after 10 h of the reaction over both CZAZOC-4 and CZAZOC-6, indicating the possible involvement of the WGS equilibrium (see Eq. [3]).

Effect of methanol injection rate. Figure 11 shows the effect of methanol injection rate or pseudo contact time on the catalytic performance. The data were collected either by adjusting the flow rate of the $CH_3OH + H_2O$ mixture or by varying the weight of the catalyst but fixing the O_2/CH_3OH molar ratio = 0.3. It can be seen that an increase in methanol injection rate increases the rate of methanol conversion and the rates of H_2, CO, and CO_2 production. The methanol injection rate can also be considered as weight hourly space velocity (WHSV) or the *inverse* of the pseudo contact times. This study is therefore useful in understanding the mechanism of the OSRM reaction. A higher methanol injection rate indicates a lower

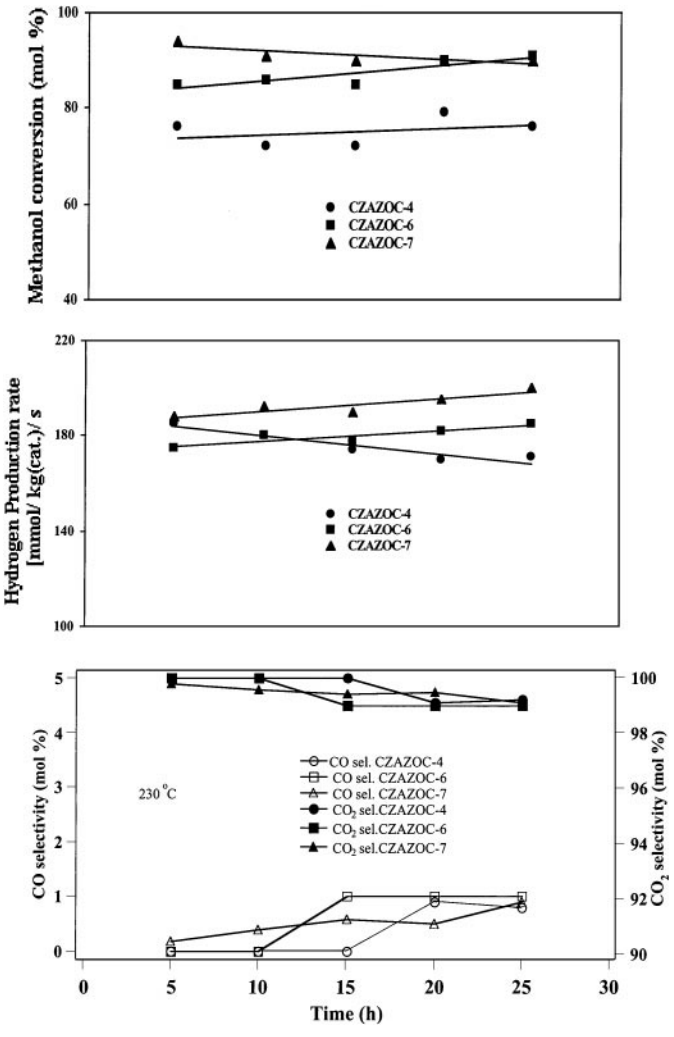

FIG. 10. Time-on-stream experimental results over CuZn-based catalyst containing only Al (CZAZOC-4), catalyst containing both Al and Zr (CZAZOC-6), and catalyst containing only Zr (CZAZOC-7) in the oxidative steam reforming of methanol reaction.

methanol contact time. It can be seen from Fig. 11C, where methanol conversion and product selectivity are plotted as a function of the *inverse* of the methanol injection rate or pseudo contact time, that both CO_2 and CO are present at shorter contact times. This indicates that CO is produced as a primary product in a parallel reaction, possibly by the decomposition of methanol,

$$CH_3OH \Leftrightarrow 2H_2 + CO \quad [5]$$

$$CO + 1/2\ O_2 \Leftrightarrow CO_2. \quad [6]$$

The CO selectivity decreases while the H_2 selectivity increases with increasing contact time. Because of the minor variations, the selectivity trend is not clearly discernable from Fig. 11C. However, from the inset of Fig. 11B, which is a plot of the CO yield and the ratio of the H_2 production rate to the $(CO + CO_2)$ production rate $[RH_2/R(CO + CO_2]$ as functions of pseudo contact time, it is apparent that the yield of CO is very high, about 1200 ppm at a contact time of 0.004 kg s $mmol^{-1}$, and it decreases to around 300 ppm with increasing contact time to about 0.02 kg s $mmol^{-1}$. Furthermore, the value $[RH_2/R(CO + CO_2]$ increases from about 2.6 to 3.2 with increasing contact time. These results indicate that the CO formed in the primary reaction is subsequently converted into CO_2 and H_2 by the WGS reaction (Eq. [3]). This observation is in agreement with the reaction mechanism proposed for the steam reforming and partial oxidation of methanol reactions over similar Cu-based catalysts (3, 15, 30, 31). In contrast, Breen *et al.* (29) and Jiang *et al.* (32) have reported that CO was formed as a secondary product by the *reverse* of the WGS reaction. However,

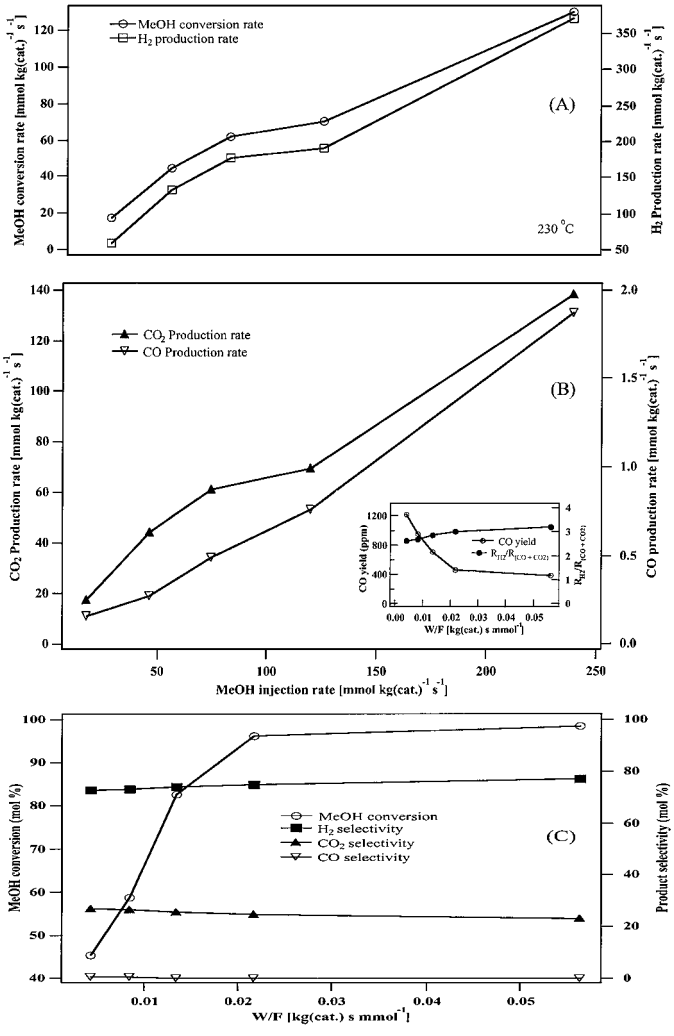

FIG. 11. Effect of methanol injection rate and pseudo contact time on the catalytic performance in the oxidative steam reforming of methanol: (A) rates of methanol conversion and H_2 production, (B) rate of carbon (CO and CO_2) formation, (C) methanol conversion and product selectivity. Inset in (B) is the variation of CO yield and the ratio of rate of H_2 production and $(CO + CO_2)$ production as a function of pseudo contact time. Results were collected using a methanizer-FID GC assembly.

under the present experimental conditions the participation of oxidation of CO into CO_2 (Eq. [6]) cannot be discarded. This is because it has been pointed out earlier (33) that in steam reforming followed by fuel gas refinement using WGS step at a temperature of approximately 200°C, it is impossible to obtain CO concentrations below 6000 ppm due to the WGS equilibrium limitations. Although, as of now we do not have direct evidence for the involvement of Eq. [6], the results of Sekizawa *et al.* (34), who have obtained a CO concentration of about 150 ppm at 150°C in combined WGS and CO oxidation reactions over similar CuZn-based catalysts downstream from the SRM reaction, support our assumption. Further experiments are currently underway to fully understand the mechanism of the OSRM reaction.

CONCLUSIONS

It is clear from the results obtained in the present study that the OSRM reaction over these novel CuZnAl(Zr)-oxide catalysts derived from hydroxycarbonate precursors containing hydrotalcite/aurichalcite phase is a very efficient and convenient method for the selective production of hydrogen. Our detailed investigation revealed that the catalyst composition has a strong influence on the physicochemical properties such as copper reducibility, surface area, and dispersion, which in turn influence the catalyst performance. The catalytic activity improved with decreasing Al content because of an enhancement in the copper reducibility, surface area, and dispersion. A part of the copper species (referred to as isolated Cu^{2+} species) in Al-rich samples is interacting with Al, and gets reduced at relatively higher temperatures. The ease of reducibility is therefore likely to be an important factor in determining the efficiency of the CuZn-based catalysts in the OSRM reaction.

CuZnZr-oxide catalyst was found to be more effective than CuZnAl-oxide catalysts in the present study, indicating that zirconia is more effective support than alumina for Cu and ZnO. These catalysts also exhibit a stable activity during on-stream operation over an extended period of time (25 h). The mechanism of the OSRM reaction seems to involve methanol decomposition and water–gas shift (WGS)/CO oxidation reactions besides the steam reforming reaction to produce H_2 and CO_2.

ACKNOWLEDGMENTS

We are grateful to Professor T. Hattori, Applied Chemistry Department, Nagoya University, for many valuable suggestions on the present research. Thanks are also due to Dr. K. Toriyama, Chemistry Department, NIRIN, for her kind help in the computer simulation of EPR spectra. S.V. and M.P.K. express their sincere gratitude to the Japan International Science and Technology Exchange Center (JISTEC) for the award of STA fellowships.

REFERENCES

1. Wigley, T. M. L., Richels, R., and Edmonds, J. A., *Nature* **379**, 241 (1996).
2. Service, R. F., *Science* **285**, 682 (1999).
3. Alejo, L., Lago, R., Peña, M. A., and Fierro, J. L. G., *Appl. Catal. A General* **162**, 281 (1997).
4. Cubeiro, M. L., and Fierro, J. L. G., *Appl. Catal. A General* **168**, 307 (1998).
5. Pepley, B. A., Amphlett, J. C., Kearns, L. M., and Mann, R. F., *Appl. Catal. A General* **179**, 21 (1999).
6. Breen, J. P., and Ross, J. R. H., *Catal. Today* **51**, 521 (1999).
7. Oetjen, H.-F., Schemidt, V. M., Stimming, U., and Trila, F., *J. Elect. Chem. Soc.* **143**, 3838 (1996).
8. Schmidt, V. M., Brockerholf, P., Hohlein, B., Menzer, R., and Stimming, U., *J. Power Sources* **49**, 299 (1994).
9. Velu, S., Suzuki, K., and Osaki, T., *Chem. Commun.*, 2341 (1999).
10. Velu, S., Suzuki, K., and Osaki, T., *Catal. Lett.* **62**, 159 (1999).
11. Velu, S., Suzuki, K., Okazaki, M., Osaki, T., Tomura, S., and Ohashi, F., *Chem. Mater.* **11**, 2163 (1999).
12. Velu, S., Suzuki, K., Kapoor, M. P., Tomura, S., Ohashi, F., and Osaki, T., *Chem. Mater.* **12**, 719 (2000).
13. Bond, G. C., and Namijo, S. N., *J. Catal.* **118**, 507 (1989).
14. Wachs, I. E., and Madix, R. J., *J. Catal.* **53**, 208 (1978).
15. Huang, H., and Wang, S., *Appl. Catal.* **24**, 287 (1986).
16. Morterra, C., Giamello, E., Cerrato, G., Centi, G., and Perathoner, S., *J. Catal.* **179**, 111 (1998).
17. Morpurgo, S., Jacono, M. L., and Porta, P., *J. Mater. Chem.* **4**, 197 (1994).
18. Indovina, V., Occhiuzzi, M., Pietrogiacomi, D., and Tuti, S., *J. Phys. Chem. B* **103**, 9967 (1999).
19. Centi, G., Perathoner, S., Bigleno, D., and Giamello, E., *J. Catal.* **151**, 75 (1995).
20. Praliand, H., Mikhailenko, S., Chajar, Z., and Primet, M., *Appl. Catal. B Environmental* **16**, 359 (1998).
21. Dow, W., Wang, Y., and Huang, T., *J. Catal.* **160**, 155 (1996).
22. Giamello, E., Fubini, B., and Lauro, P., *Appl. Catal.* **21**, 133 (1986).
23. Martinez-Arias, A., Cataluña, R., Conesa, J. C., and Soria, J., *J. Phys. Chem. B* **102**, 809 (1998).
24. Fujitani, T., and Nakamura, J., *Catal. Lett.* **56**, 119 (1998).
25. Fisher, I. A., and Bell, A. T., *J. Catal.* **172**, 222 (1997).
26. Fisher, I. A., and Bell, A. T., *J. Catal.* **178**, 153 (1998).
27. Fisher, I. A., and Bell, A. T., *J. Catal.* **184**, 357 (1999).
28. Fierro, G., Jacono, M. L., Inversi, M., Prta, P., Cioci, F., and Lavecchia, R., *Appl. Catal. A General* **137**, 327 (1996).
29. Breen, J. P., Meunier, F. C., and Ross, J. R. H., *Chem. Commun.*, 2247 (1999).
30. Amphlett, J. C., Creber, K. A., Davis, J. M., Mann, R. F., Peppley, B. A., and Stocks, D. M., *Int. J. Hydrogen Energy* **19**, 131 (1994).
31. Wiese, W., Emonts, B., and Peters, R., *J. Power Sources* **84**, 187 (1999).
32. Jiang, C. J., Trimm, D. L., Wainwright, M. S., and Cant, N. W., *Appl. Catal. A General* **97**, 81 (1994).
33. Höhlein, B., Boe, M., Bøgild-Hansen, J., Bröckerhoff, P., Colsman, G., Emonts, B., Menzer, R., and Riedel, E., *J. Power Sources* **61**, 143 (1996).
34. Sekizawa, K., Yano, S., Eguchi, K., and Arai, H., *Appl. Catal. A General* **169**, 291 (1998).